

Above-ground biomass change estimation using national forest inventory data with Sentinel-2 and Landsat

S. Puliti^{a,*}, J. Breidenbach^a, J. Schumacher^a, M. Hauglin^a, T.F. Klingenberg^b, R. Astrup^a

^a Norwegian Institute for Bioeconomy Research (NIBIO), Division of Forest and Forest Resources, National Forest Inventory, Høgskoleveien 8, 1433 Ås, Norway

^b Norwegian Mapping Authority (Kartverket), Land Mapping Division, P.O. Box 600, Sentrum, 3507 Hønefoss, Norway



ARTICLE INFO

Edited by: Marie Weiss

Keywords:

Forest carbon dynamics
Satellite imagery
greenhouse-gas reporting
model-assisted estimation

ABSTRACT

This study aimed at estimating total forest above-ground net change (ΔAGB ; Gg) over five years (2014–2019) based on model-assisted estimation utilizing freely available satellite imagery. The study was conducted for a boreal forest area (approx. 1.4 Mha) in Norway where bi-temporal national forest inventory (NFI), Sentinel-2, and Landsat data were available. Biomass change was modelled based on a direct approach. The precision of estimates using only the NFI data in a basic expansion estimator was compared to four different alternative model-assisted estimates using 1) Sentinel-2 or Landsat data, and 2) using bi- or uni-temporal remotely sensed data.

We found that spaceborne optical data improved the precision of the purely field-based estimates by a factor of up to three. The most precise estimates were found for the model-assisted estimation using bi-temporal Sentinel-2 (standard error; SE = 1.7 Gg). However, the decrease in precision when using Landsat data was small (SE = 1.92 Gg). We also found that ΔAGB could be precisely estimated when remotely sensed data were available only at the end of the monitoring period.

We conclude that satellite optical data can considerably improve ΔAGB estimates, when repeated and coincident field data are available. The free availability, global coverage, frequent update, and long-term time horizon make data from programs such as Sentinel-2 and Landsat a valuable data source for consistent and durable monitoring of forest carbon dynamics.

1. Introduction

Forests play a central role in regulating the global climate through processes such as carbon uptake, carbon emission, and the regulation of the water and energy cycles (Herold et al., 2019). Forest structures are dynamic systems varying through space and time. Understanding the dynamics of the forest above-ground biomass (AGB) is critical to better comprehend the impact of forest management on climate change (Duncanson et al., 2021; Eggleston et al., 2006). Repeated national forest inventory (NFI) data, along with freely available medium-resolution satellite imagery such as Sentinel-2 (Drusch et al., 2012) or Landsat data (Wulder et al., 2012), offer unique possibilities for long-term monitoring of AGB dynamics (GFOI, 2020). Such medium-resolution satellite data are available at a global scale and at high temporal resolution (5–16 days at the equator). These missions are planned to span across several decades, making them one of the most useful source of auxiliary information for national and international

forest monitoring programs. Despite the current need for globally consistent estimates of forest AGB dynamics (Duncanson et al., 2019), little is known about satellite optical data's contribution to AGB change estimation in the context of green-house gases inventories.

1.1. Remotely sensed based ΔAGB estimation

During the past decade, the majority of the studies aimed at developing methods to map and estimate AGB stocks at specific points in time (Zolkos et al., 2013). Only a minority of studies looked at the use of multi-temporal remotely sensed data for estimating and mapping AGB change (ΔAGB). As a prominent source of auxiliary information for AGB estimation and mapping, airborne laser scanning (ALS) data has been found useful also in improving the precision of ΔAGB estimates based on field reference data alone by factors of 2–9 (Bollandsås et al., 2018; McRoberts et al., 2015; Næsset et al., 2013; Næsset et al., 2015; Skowronski et al., 2014). Other three-dimensional remotely sensed data, such

* Corresponding author.

E-mail address: stefano.puliti@nibio.no (S. Puliti).

as digital aerial photogrammetry, have been found useful to fit nationwide ΔAGB models (Price et al., 2020). Even though such three-dimensional remotely sensed data represent the state-of-the-art, their use remains limited in terms of large area coverage due to prohibitive acquisition costs.

When aiming at producing consistent estimates on a continental or even global scale, satellite data represent a more cost-efficient and thus promising data source for the estimation of ΔAGB over extended periods (GFOI, 2020). New and upcoming scientific satellite missions such as the GEDI and ESA's BIOMASS have been specifically tailored to the need for improving our understanding of near-global forest biomass stocks (Duncanson et al., 2019). Even though such missions may improve our understanding of the present state of forest AGB stocks, they remain characterized by short lifespans (2–5 years) and do not cover the entire globe. Amongst the past experiences, both interferometric synthetic aperture radar (InSAR) (Karila et al., 2019; Solberg et al., 2014) and optical data (Main-Knorn et al., 2013; Powell et al., 2010), such as TanDEM-X and Landsat multi-temporal data have been used to map ΔAGB . InSAR data has the advantages of being cloud-insensitive and allowing the 3D characterization of the forest canopy height. Nevertheless, the commercial nature of available InSAR data suitable for forest AGB estimation (e.g. TanDEM-X), limits their use across space and time. While freely available Sentinel-1 InSAR data could be of interest, their use has only been tested for mapping AGB stocks (Laurin et al., 2018; Li et al., 2020) and no study has yet assessed the use of Sentinel-1 for AGB change mapping and estimation.

Amongst the broad panorama of the currently available remotely sensed data, medium-resolution (10–30 m) optical data represents one of the most promising sources of auxiliary data as they allow virtually anyone to access near-real-time as well as archive imagery over any point on earth and free of cost. The long term lifespan of these missions makes them particularly suitable for continuous monitoring of forest AGB dynamics.

1.2. ΔAGB using open satellite optical data

In the realm of optical data, time series of reflectance data from Landsat have been and continue to be effectively used to monitor the global extent and patterns of forest cover disturbance and recovery (Cohen et al., 2010; Hansen et al., 2013; White et al., 2018). Concerning the quantification of the carbon uptake and emission, methods to estimate AGB losses from carbon density maps have been proposed (Baccini et al., 2012; Csillik et al., 2019). While such maps may be used to quantify forest carbon emissions, they lack information on the carbon sequestration potential and thus the net ΔAGB . Only a handful of studies used time-series of Landsat data to model AGB over time and consequently derive AGB changes (Main-Knorn et al., 2013; Matasci et al., 2018; Nguyen et al., 2020; Powell et al., 2010; Wulder et al., 2020). Even though useful to characterize areal changes based on the loss or accumulation of forest AGB, the previously proposed methods lacked a rigorous assessment of the uncertainty of the ΔAGB estimates and thus do not comply with guidelines for estimation of emissions and removals of greenhouse gasses in forests indicated by the Global Forest Observation Initiative GFOI (2020). Knowledge of the ΔAGB estimates' uncertainty is essential for current green-house gasses inventories, and according to good practice, the estimates should be neither systematically over- nor under-estimating the true ΔAGB and they should be precise so far as practicable (IPCC 2019). To meet these criteria, it is thus important to adopt unbiased estimators and to report the uncertainty of an estimate, without which it is not possible to assess the precision of an estimate.

1.3. Methods for change estimation

In forest inventories supported by remotely sensed data, the estimation of ΔAGB and its uncertainty may be done either through model-

assisted or model-based estimators (Gregoire, 1998; Ståhl et al., 2016). Both rely on the use of models linking field reference data with remotely sensed auxiliary data to improve the precision of purely field-based estimates. The model-assisted estimator is preferred when a probability sample of field observations is available as it is nearly-unbiased even if the model has a lack of fit (Särndal, 1984).

Concerning the models used, ΔAGB may be estimated either using a direct or indirect modeling approach (McRoberts et al., 2015). The former consists in directly modeling ΔAGB , while the latter consists in modeling AGB state in the two points in time (T_1 and T_2) separately and estimating ΔAGB as the difference between the AGB in T_2 and the AGB in T_1 . When repeated and coincident field plot data are available, the direct approach is often preferred as it relies on a single model and thus a single error source (Bollandsås et al., 2013; Fuller et al., 2003; McRoberts et al., 2015; Skowronski et al., 2014). Within the direct approach, one may consider using either bi-temporal or only uni-temporal remotely sensed data. The use of the bi-temporal approach represents a familiar approach (Bollandsås et al., 2018; McRoberts et al., 2015; Næsset et al., 2015), which intuitively relies on the temporally matching field and remotely sensed data in both T_1 and T_2 . The uni-temporal approach is representative of those cases when remotely sensed data are available only for T_2 . Thus, AGB changes are explained only as a function of a snapshot (e.g., satellite image) at the end of the monitoring period. While unexplored, this approach is relevant for satellite optical data in those cases without available images in T_1 due to cloud-cover or to the fact that the satellite was not even launched. Direct ΔAGB models relying on uni-temporal remotely sensed data could broaden the time window available for estimating ΔAGB and thus provide an understanding of past forest AGB dynamics.

1.4. Field reference data

An important limiting factor to direct ΔAGB modeling lies in the lack of repeated and coincident field reference data at different times (Næsset et al., 2015). Consequently, the gain-loss method often represents the only solution (GFOI, 2013; McRoberts et al., 2020). Continuously updated NFIs represent a unique data source to estimate ΔAGB based on a stock-difference method. As an example, the Norwegian NFI is composed of a systematic network of more than 22,000 permanent field plots. Every five years, a fifth of the plots are re-measured, allowing to estimate ΔAGB over the past five years period (Breidenbach et al., 2020a). The scope of NFIs is mainly to provide nationwide and regional statistic, however they can also provide an important contribution to global efforts to monitor forest carbon dynamics. The availability of nationwide, repeated, and geolocated AGB observations offers unique possibilities for the direct estimation of ΔAGB using satellite optical data.

1.5. Study objective

Our study is part of the ongoing global research effort aiming on improving methods for reliable and consistent greenhouse gas inventories in order to fully understand and utilize the climate mitigation potential of forests (e.g., Harris et al., 2021). The objective of this study was to compare the precision of ΔAGB estimates for a period of five years (2014–2019 or 2010–2015) using bi-temporal NFI data and either bi-temporal ($T_1 = 2015$ and $T_2 = 2019$) or uni-temporal ($T_2 = 2019$ or 2015) Sentinel-2 or Landsat data. Direct estimates of the total net ΔAGB were obtained according to a model-assisted estimator, and the results compared to estimates based on a basic expansion estimator (BE) using the NFI data alone.

2. Materials

2.1. Study area

The study area was in south-eastern Norway and comprised a total area of 13,659 km² (see Fig. 1). This specific area was selected as it was one of the largest contiguous areas in Norway where Sentinel-2 data were available and free of cloud cover during 2015, which was also the first year that the Sentinel-2 A satellite was operational (i.e., limited number of images). The forest area estimated using all NFI plots within the AOI is nearly 70% of the total area. The AOI is characterized by a large proportion of forest (nearly 70%) actively managed for timber production. The forest composition was typical of boreal forest characterized by a prevalence of coniferous species (88%). In our study area, the dominant species was *Picea abies* (67%), followed by *Scots pine* (21%), and deciduous species (12%). With the absence of substantial forest fires or insect outbreaks in the study area, forest harvest represents the primary source of disturbance.

2.2. National Forest Inventory data

The Norwegian NFI is based on a five-year repeat cycle according to which a fifth of the plots are visited annually (Breidenbach et al., 2020a). The permanent plots were established in 1986–1993 and since 1994, one fifth of the plots are re-measured in a regular five-year cycle. The availability of repeated and coincident field plot data allows the calculation of plot-wise ΔAGB (Mg ha⁻¹) as the difference between the AGB stock at the end (T_2) and the beginning of the monitoring period (T_1). Permanent NFI field plots are systematically located in a 3 × 3 km

grid within the study area. The set of field plots measured each year is selected based on a Latin-square design, resulting in evenly distributed clusters of 3 × 3 field plots measured each year (Fig. 1). The permanent field plots from the five-year cycles 2010–2015 and 2014–2019 were used in the present study.

2.2.1. AGB estimation on the NFI field plots

Within the 250 m² circular field plots, the diameter at breast height (DBH) of trees with DBH ≥ 5 cm was recorded. Tree height was measured on selected trees, according to the NFI field protocol (Breidenbach et al., 2020a). Field measurements from 2014 and 2019 were then used with species-specific allometric models to estimate AGB for each field plot at T_1 and T_2 , respectively (Marklund, 1988). Each field plot's center point was positioned using a Global Navigation Satellite System receiver, allowing for spatial alignment with satellite data.

Further details about the field registrations in the Norwegian NFI can be found in (Breidenbach et al., 2020a).

2.3. Remotely sensed data

2.3.1. Sentinel-2

Atmospherically corrected Sentinel-2 (level 2A) cloud-free mosaics were generated for two points in time: summer 2015 and summer 2019. The mosaics were generated using images from August 2 to August 22 in 2015 and between July 27 and September 20 in 2019. While optimally, the remotely sensed data should be temporally matching the field reference data in 2014 and 2019, the first Sentinel-2 images were available only in 2015. Since Sentinel-2 L2A scenes were not systematic in production before May 2017, Sentinel-2 Level-1C scenes in 2015 were

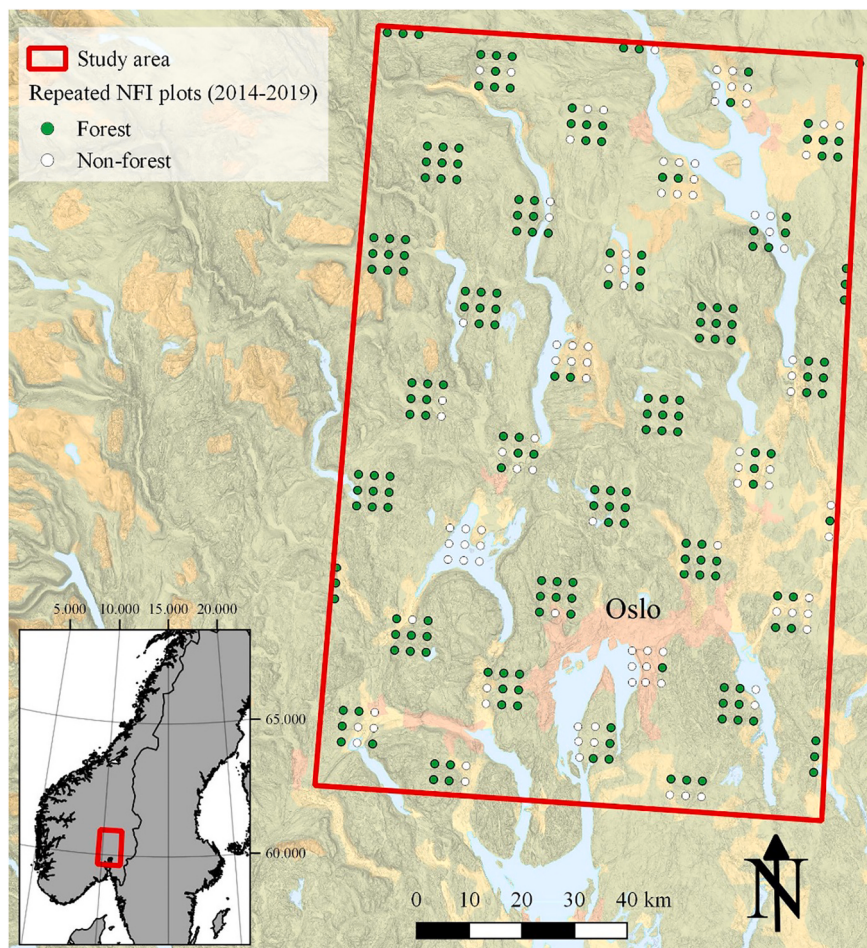


Fig. 1. Overview of the study area, highlighting the NFI sampling design for the permanent plots measured in 2014 and 2019.

atmospherically corrected, using the Sen2Cor processor version 2.8 (Gascon et al., 2017).

The acquired 2015 Sentinel-2 L1C and 2019 Sentinel-2 L2A scenes were downloaded from the Copernicus Open Access Hub (Copernicus, 2020). The mosaics contained the bands 2 through 8, 8A, 11, and 12 (see Table 1), and was created by the following steps: for each Sentinel-2 L2A scene, we created a single PCI Geomatics file containing the bands mentioned above. Bands with 20 m resolution were resampled to 10 m with nearest neighbor resampling. Then within the AOI, polygons were manually drawn over clouds and cloud-shadows and replaced with cloudless scenes. The mosaicking was done in the PCI Geomatics Mosaic Tool, and we used dodging-points for color balancing, including contrast and brightness adjustment, to derive seamless mosaics. A dodging point is a focal point on which we can adjust the color balancing. We used them only in cases of substantial differences in the reflectance of two adjacent acquisition dates. This method, also used in the study by Puliti et al. (2020), was adopted as it is part of the processing pipeline used by the Norwegian mapping Authority for the yearly production of nationwide Sentinel-2 mosaics. While services such as the Copernicus Sentinel-2 global mosaic (Copernicus, 2020b) allow for producing consistent cloud free mosaics anywhere on the globe, and would therefore be a suitable data source for this study, no such data were available for 2015. For each of the NFI plots, we extracted the Sentinel-2 band values corresponding with the plot center's coordinates.

2.3.2. Landsat

Landsat Analysis Ready Data produced by the Global Land Analysis and Discovery team at the University of Maryland (GLAD ARD, Potapov et al., 2020) were used as a source of yearly cloud-free Landsat mosaics. For comparison with the Sentinel-2 data, we selected mosaics from the same two points in time (i.e., 2015 and 2019). These data represent a globally available data source for long term monitoring (1997–present) of land cover change mapping. GLAD ARD data are produced by drawing upon the entire archive of Landsat data from 1997 to present and by selecting the imagery with highest geometric and radiometric standards (GLAD ARD, Potapov et al., 2020). The GLAD ARD data are produced consistently at a global scale, making them particularly suitable for ensuring the reproducibility of the estimates.

The cloud-free mosaics of normalized surface reflectance from Landsat data were generated using the phenological metrics type A in the GLAD tools for Landsat ARD applications (Glad, 2020). The mosaics are gap-filled to remove clouds, snow, and shadows. Each composite represents the average reflectance values between the 25th and 75th percentile from the gap-filled cloud-free annual observation time-series.

Specific details of the processing steps involved in GLAD ARD data production can be found in Potapov et al. (2020). As for the Sentinel-2 data, the bands' values corresponding to each NFI plot centre were extracted.

Table 1
Spectral bands (nm) and resolution (m) for the Sentinel-2 and Landsat imagery.

Band number ^a	Sentinel-2	Landsat
B2	Blue (458–523 nm) 10 m	Blue (452–512 nm) 30 m
B3	Green (543–578 nm) 10 m	Green (533–590 nm) 30 m
B4	Red (650–680 nm) 10 m	Red (636–673 nm) 30 m
B5	Red-edge 1 (698–713 nm) 20 m	NIR (851–879 nm) 30 m
B6	Red-edge 2 (733–748 nm) 20 m	SWIR 1 (1566–1651 nm) 30 m
B7	Red-edge 3 (773–793 nm) 20 m	SWIR 2 (2107–2294 nm) 30 m
B8	NIR 1 (785–899 nm) 10 m	–
B8A	NIR 2 (855–875 nm) 20 m	–
B11	SWIR 1 (1565–1655 nm) 20 m	–
B12	SWIR 2 (2100–2280 nm) 20 m	–

^a The band numbers reported for Sentinel-2 and Landsat data correspond to the original order for the respective sensors as described in their respective official documentation.

2.3.3. Forest mask

A nationally available forest mask was used to define the population of interest geographically. The forest mask is based on the Norwegian land capability classification system, “AR5” (Ahlstrøm et al., 2014) and is currently used for the nationwide mapping of forest resources in Norway (Astrup et al., 2019). While dating back to the 1960s, such a forest mask currently represents the best source of information on the extent and spatial distribution of forests in Norway with an accuracy of 92% (Breidenbach et al., 2020b). The forest mask is produced from the field and aerial surveys and is currently updated based on ALS data.

3. Methods

The workflow consists of five steps (Fig. 2), consisting in 1) processing the remotely sensed and NFI field data, 2) extracting the predictor variables from Sentinel-2 and Landsat for each NFI plot and for each point in time; 3) modeling the response ΔAGB according to a direct approach using the predictor variables extracted from either uni- or bi-temporal satellite imagery; 4) applying the developed models to the entire forest population; 5) estimating the total ΔAGB and its uncertainty according to model-assisted inference. The performance of the method was benchmarked against a basic expansion estimator using only NFI plot data and no remotely sensed data.

3.1. Modeling ΔAGB

To model ΔAGB , we opted for a direct method according to which the remotely sensed auxiliary variables are used to model the change in AGB in the NFI plots directly. Two different approaches to modeling ΔAGB , namely:

- 1. **Bi-temporal:** such an approach consisted of using explanatory variables from Sentinel-2 and Landsat data from both points in time (2015 and 2019).
- 2. **Uni-temporal:** this approach assumed that remotely sensed data were available only for T_2 and thus links AGB changes to the reflectance properties of the forest at a single step in time. The uni-temporal approach was applied both to estimate changes in the periods 2010–2015 and 2014–2019.

The models were fitted using explanatory variables independent of pairing, meaning that the bands selected for T_1 are not necessarily selected for T_2 and vice versa. This model form was adopted as it was found to yield the most precise estimates in a comparative study of several different model forms by McRoberts et al. (2015). Using only the plots classified as forest in the NFI data, we fitted four separate multiple linear models linking the ΔAGB from the NFI data with bi-temporal or uni-temporal data either from Sentinel-2 or Landsat. The explanatory variables consisted of the bands' values as well as band indices. Similarly to the normalized difference vegetation index (NDVI), the band indices were calculated as the ratio between the difference and the sum of band pairs. We calculated the band indices from all band combinations (i.e., 45 and 15 combinations for Sentinel-2 and Landsat for each point in time).

The predictor variables were selected to ensure parsimonious models and avoid multicollinearity. First, we performed a branch-and-bound search for the best subset based on the Bayesian information criterion. Second, the models were penalized for multicollinearity by ensuring that the largest variance inflation factor was less than five.

3.2. Estimation

An estimate of the total forest net ΔAGB ($\hat{\tau}$) and its variance ($\widehat{\text{Var}}(\hat{\tau})$) using a basic expansion (BE) estimator just based on field data and a model-assisted (MA) estimator were calculated as presented in the

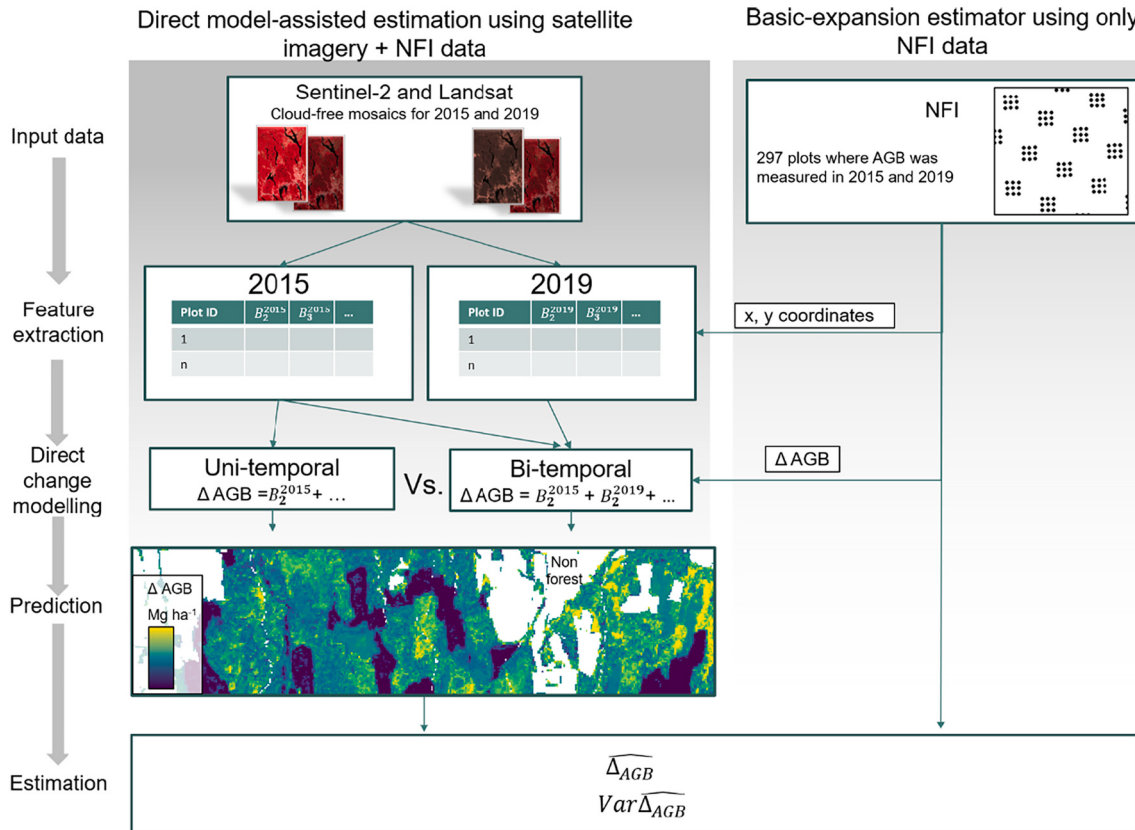


Fig. 2. Flowchart illustrating the different steps adopted to obtain estimates of ΔAGB and its uncertainty using either a model-assisted or a basic expansion estimator.

following.

We assumed the field reference data (S) to be a simple random sample of size n , resulting in the BE estimator of the total

$$\widehat{\tau}_{BE} = \frac{A}{n} \sum_{i \in S=1}^n y_i \quad (1)$$

where $A = 1,342,397$ ha is the total land area of the study area, and y_i is the ΔAGB over five years ($Mg ha^{-1}$), for the i th NFI field plot ($i = 1, \dots, n$). The variance of the total was estimated by

$$\widehat{Var}(\widehat{\tau}_{BE}) = \frac{S^2}{n} A^2 \quad (2)$$

where S^2 is the sample variance

$$S^2 = \frac{1}{n-1} \sum_{i=1}^n (y_i - \bar{y})^2 \quad (3)$$

and \bar{y} is the sample mean.

For MA estimation, the ΔAGB models devised in sub-section 2.4.1 using bi- or uni-temporal data from Sentinel-2 or Landsat data were applied to each pixel in the study area. The pixel-predictions were then masked using the available forest mask to exclude non-forest areas resulting in a synthetic estimate of ΔAGB . Furthermore, a binary indicator variable I defined whether the plot was forested ($I=1$) or not ($I=0$) according to the NFI. The MA estimator of total ΔAGB was

$$\widehat{\tau}_{MA} = A \frac{1}{N} \sum_{k=1}^N \widehat{y}_k + A \frac{1}{n} \sum_{i=1}^n \varepsilon_i \quad (4)$$

where \widehat{y}_k are pixel-level ΔAGB predictions, N is the number of pixels within the forest mask and ε_i is the residual

$$\varepsilon_i = y_i - (\widehat{y}_i I_i) \quad (5)$$

where \widehat{y}_i is the plots' predicted ΔAGB and I_i the indicator variable. The first component of eq. 4 represents the synthetic (map-based) estimator, and the second component is an estimated correction factor. The MA variance was estimated according to

$$\widehat{Var}(\widehat{\tau}_{MA}) = \frac{A^2}{n(n-1)} \sum_{i=1}^n (\varepsilon_i - \bar{\varepsilon})^2 \quad (6)$$

where $\bar{\varepsilon}$ is the mean residual.

Finally, the BE and MA estimates were compared by the relative efficiency (RE), calculated as the ratio $\widehat{Var}(\widehat{\tau}_{BE}) / \widehat{Var}(\widehat{\tau}_{MA})$ where the latter was estimated either using Sentinel-2 or Landsat data. The RE was used to describe the relative improvement in the model-assisted estimates' precision over the direct estimates. As the study population included only forest areas, the ΔAGB for plots outside forest areas (according to the NFI classification) was set to zero (Breidenbach et al., 2020b).

4. Results and discussion

4.1. Models

The bi-temporal Sentinel-2 model (see sub-section 2.4.1) included the index between the red-edge 3 (B7) and SWIR 2 (B12) in 2015 and 2019 (Table 2). The selection of the same pair of bands in bi-temporal Sentinel-2 data is intuitive as it allows to link changes in AGB to changes in reflectance. On the other hand, the selected variables in the Landsat bi-temporal model were not paired and included the blue (B2) from 2015, and the red (B4) and the NIR band (B7) for 2019. The

Table 2
Summary of the ΔAGB models for Sentinel-2 and Landsat.

Period of interest	Auxiliary data	Model type	model	Adj. R ²
2014–2019	Sentinel-2	Bi-temporal	$\Delta\text{AGB} = -79.86 - 137.32 B_{7/12}^{2015} + 284 B_{7/12}^{2019}$	0.64
		Uni-temporal	$\Delta\text{AGB} = -185.93 - 485.72 B_{4/7}^{2019} + 301.76 B_{4/11}^{2019}$	0.61
	Landsat	Bi-temporal	$\Delta\text{AGB} = -32.53 + 0.071 B_2^{2015} - 0.050 B_7^{2019} - 94.69 B_{4/7}^{2019}$	0.56
		Uni-temporal	$\Delta\text{AGB} = -0.04 + 0.0095 B_5^{2019} - 0.04 B_7^{2019}$	0.46
2010–2015	Sentinel-2	Uni-temporal	$\Delta\text{AGB} = -108.9 + 198.9 B_{6/12}^{2015}$	0.25
	Landsat	Uni-temporal	$\Delta\text{AGB} = 36.34 + 0.0068 B_5^{2015} - 0.0189 B_6^{2015}$	0.24

Sentinel-2 and Landsat variables in T_2 were more strongly correlated to ΔAGB than those in T_1 , justifying the adoption of a uni-temporal approach. The maximum correlations were $r = -0.65$ for Sentinel-2 SWIR2 and $r = -0.6$ for Landsat's SWIR2 in T_2 and $r = -0.15$ for Sentinel-2 red and $r = -0.06$ for Landsat's SWIR2 band in T_1 . When using only satellite optical data from T_2 , the Sentinel-2 model included the ratio between the red (B4) and the red-edge 3 (B7), and the ratio between the red and a SWIR1 band (B11). The Landsat uni-temporal model included the NIR (B5) and a SWIR 2 (B7).

For the period 2014–2019, the Sentinel-2 models had better model fit

(Adj.R² = 0.61–0.64) than the Landsat ones (Adj.R² = 0.46–0.56). The uni-temporal data was characterized by a greater decrease in the model's explanatory power than bi-temporal data. Compared to previous studies adopting a direct modeling approach for ΔAGB estimation in boreal forests, the models devised in this study performed better than InSAR data (R^2 in the range 0.2–0.6) (Næsset et al., 2015) and ALS data in montane forests ($R^2 = 0.28$) (Bollandsås et al., 2018). On the other hand the model fit was poorer than what was previously found when using ALS data in productive forests (i.e., Adj. R² in the range 0.6–0.9) (McRoberts et al., 2015; Næsset et al., 2013). While ALS data are the state-of-the-art source of auxiliary information for forest AGB modeling, its large acquisition costs make it unsuitable for long-term, continuous, and nationwide AGB monitoring programs.

Interestingly, the uni-temporal ΔAGB models using Sentinel-2 or Landsat data for the period 2010–2015 had a notably poorer fit (Adj.R² = 0.24–0.25) compared to the 2014–2019 models (Adj.R² = 0.41–0.61). In addition to variations in the quality of the satellite image mosaics in 2015 band 2019, important factors explaining this decreased model performance relate to the differences in harvest extent and intensity, and in the NFI sample plots available for the two studied periods. During the 2010–2015 period, only 20 NFI plots had a negative ΔAGB , compared to 33 in the 2014–2019 period. Along with an increase in harvested area, the available NFI data revealed an increase in the magnitude of the removals between the 2010–2015 ($-59.42 \text{ Mg ha}^{-1}$ on average) and the 2014–2015 period ($-70.15 \text{ Mg ha}^{-1}$ on average). These figures suggest that the quality of the model fit is somewhat related to the number of

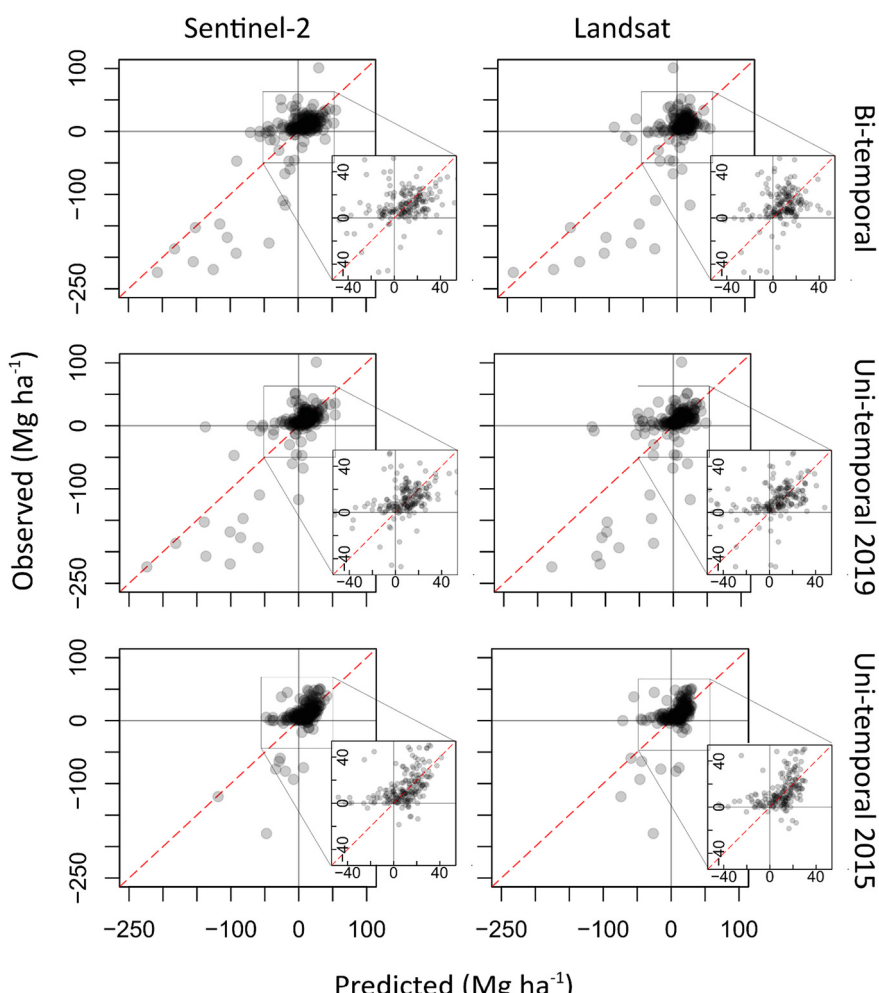


Fig. 3. Observed (NFI) vs. predicted ΔAGB using either Sentinel-2 or Landsat data and using bi-temporal data or uni-temporal data. The perpendicular lines represent the 0,0 origin, and the dashed line is the 1:1 line. The inset scatterplots show a detail between -50 Mg ha^{-1} and 50 Mg ha^{-1} .

available field plots with AGB losses and the magnitude of those losses.

The analysis of the predictions of the Sentinel-2 models (see Fig. 3) revealed a general tendency of to under-predict the ΔAGB in plots characterized by AGB losses. The Sentinel-2 and the Landsat based ΔAGB predictions were negative for 84% and 69% of the plots with observed AGB loss. As visible in the detailed scatterplots around $\pm 50 \text{ Mg ha}^{-1}$ in Fig. 3, most of the observations consisted in subtle AGB gains.

While the scope of this study was to estimate net AGB changes, Table 3 shows that the coefficient of determination (R^2) between the NFI ΔAGB and the models' predictions was on average larger for plots with AGB loss ($R^2 = 0.43$) compared to plots with AGB gains ($R^2 = 0.17$). Such figures indicate a limited ability of the model to support the estimation of the gains due to the small magnitude of the gains and the difficulty to derive reflectance features that can properly explain different forest growth patterns. This highlights an important challenge in fitting a single model to data characterized by AGB gains and losses. In managed boreal forests, due to the slow growth of the forest, the gains are generally of smaller magnitude than the losses, which in contrast are mostly abrupt losses of large AGB stocks due to full harvest of the trees.

An example of the predictions for the bi-temporal Sentinel-2 data is shown in Fig. 4. It is possible to clearly identify harvested areas and different growth rates in forests with different developmental stage. Unlike previous studies on direct ΔAGB estimation (McRoberts et al., 2015; Næsset et al., 2013), no truncation of the models' predictions was deemed necessary. Only 0.6% and 1.4% of the Sentinel-2 and Landsat pixels respectively were outside the range of values in the sample. To further use the models devised in this study for estimation purposes, we reported the variance-covariance matrices in Annex 1.

4.2. Estimation

The BE estimate of ΔAGB based exclusively on NFI data was 0.12 Gg with a $\text{SE} = 2.94 \text{ Gg}$ (Table 4). For the studied period, the ΔAGB was smaller than any of the previous five-years NFI cycles from 2010 until 2018 (see Fig. 4). This was mainly due to a larger number of plots with AGB loss during the studied period (2014–2019) compared to the earlier periods. Compared to previous studies conducted on a smaller scale in Norway using airborne laser scanning, our estimate of the average yearly ΔAGB ($0.03 \text{ Mg ha}^{-1} \text{ year}^{-1}$) was smaller than the one reported by Næsset et al. (2013) (2000–2010 period; $1.78 \text{ Mg ha}^{-1} \text{ year}^{-1}$), by Bollandsås et al. (2018) (2008–2012 period; $0.21 \text{ Mg ha}^{-1} \text{ year}^{-1}$), and by Strømbu et al. (2017) (2006–2011 period; $1.27 \text{ Mg ha}^{-1} \text{ year}^{-1}$). Even though the above-mentioned studies were conducted in different areas and for different periods, their estimates were of similar magnitude as the BE estimates for the period 2010 and 2019 in this study (see Fig. 5).

The model-assisted estimates of the total ΔAGB using the bi-temporal model were of 2.57 Gg ($\text{SE} = 1.7 \text{ Gg}$) and 1.83 Gg ($\text{SE} = 1.92 \text{ Gg}$) when using either Sentinel-2 and Landsat, respectively (see Table 4). When using uni-temporal data to estimate ΔAGB in the 2014–2019 period, the uncertainty of the estimates increased both for Sentinel-2 ($\text{SE} = 1.84 \text{ Gg}$) and Landsat ($\text{SE} = 2.16 \text{ Gg}$), with the latter being characterized by a larger change. While all the model-assisted estimates for total ΔAGB were larger than the direct estimate, they were well within its 95% confidence interval (see Fig. 5) and thus not significantly different from

the direct estimate. On the other end, none of the estimates were significantly different from zero at 95% confidence level and the direction of the change could only be determined at 85% and 65% confidence levels for Sentinel-2 and Landsat data, respectively. For the BE estimates, the direction of the change could be determined at a confidence level of only 3%. In line with a previous study by Ene et al. (2017), our results reflect an important challenge in estimating ΔAGB in situations where the magnitude of ΔAGB is small which requires very precise estimates to allow for determining the direction of the change with sufficient confidence. In our specific case, the small magnitude of the estimated ΔAGB could be mainly attributed to an active management of the forests for timber production with the removals approximately equaling the forest growth.

Because the estimators used in this study were either unbiased or nearly unbiased (Särndal, 1984), the point estimates' differences can be attributed to random variations (McRoberts et al., 2015). A potential reason behind such variations may be due to the nature of the satellite cloud-free mosaics, which, by blending multi-date imagery, are characterized by heterogeneous sun-target-sensor geometry and atmospheric conditions. This variation is further exacerbated when using bi-temporal mosaics due to the compound effect of random variations in reflectance from two points in time.

In this study, Sentinel-2 data for T1 were available only from 2015, and thus the temporal mismatch between the NFI data collection in 2014 and the remotely sensed data may have caused a reduction in the detectable AGB losses. While this temporal mismatch may be a drawback of this study, model-assisted estimates based on Landsat data from 2014 and 2019 (2.38 Gg ; $\text{SE} = 1.89 \text{ Gg}$) were of similar magnitude and without an appreciable increase in precision compared to when using Landsat data from 2015 and 2019. Such a result shows the viability of the proposed method even when the remotely sensed data does not perfectly match the timing of the field reference data acquisition. This characteristic may be particularly attractive for passive optical data as it allows to draw satellite images from a broader time window, thus increasing the chances of having a pair of cloud-free mosaics.

The relative efficiency (RE) of the MA estimates was 2.7 and 2.3 for the estimates using bi-temporal data and either the Sentinel-2 or the Landsat data, respectively (see Table 5). This translates into the need for nearly three times the number of NFI plots to obtain the same accuracy level as for the model-assisted estimate based on Sentinel-2 data. The relative efficiency found in this study was smaller than the range in REs reported by Næsset et al. (2013), Næsset et al. (2015), and McRoberts et al. (2015) for the direct model-assisted estimation of ΔAGB over 10 years using ALS data (RE = 3.1–10). When compared to the RE for InSAR data, our study found a larger RE than an earlier study by Næsset et al. (2015), where the RE was in the range of 1.8–2.5. Regarding the uni-temporal estimates, during the 2014–2019 period there was a decrease in RE when using uni-temporal instead of bi-temporal data. The decrease in RE was larger for Landsat (21%) than for Sentinel-2, for which the RE was only 7% smaller than when using bi-temporal data. For the 2010–2015 period the RE was only 1.3, representing a 30%–50% reduction compared to the uni-temporal estimated for the 2014–2019. Such large variability in the precision of the ΔAGB estimates through time may be due to factors related either with the quality of the remotely sensed data or the activity data. Based on the high quality of the Sentinel-2 mosaics used in this study, which were produced using single date imagery covering most of the study area (2015 and 2019), we can attribute a good portion of the decreased precision to the fact that in the 2010–2015 there was less forest harvesting activity in the study area. In line with the better model fit to NFI plots with AGB loss compared to gain plots (see Table 3), these results suggest that the precision of the estimates increases with the level and intensity of forest harvesting, which was also observed by Breidenbach et al. (2021) for carbon-stock losses. The better performances may be driven by a stronger signal (i.e. steeper AGB change) which can also be more easily detected in satellite imagery (i.e. harvested areas) compared to slow

Table 3

Coefficient of determination (R^2) of the models' ΔAGB and AGB gains and losses using either Sentinel-2 or Landsat data for each of the studied periods.

Remotely Sensed data	2014–2019		2010–2015	
	Bi-temporal		Uni-temporal	
	gain	loss	gain	loss
Sentinel-2	0.13	0.62	0.19	0.51
Landsat	0.04	0.57	0.14	0.35
			0.32	0.23
			0.24	0.33

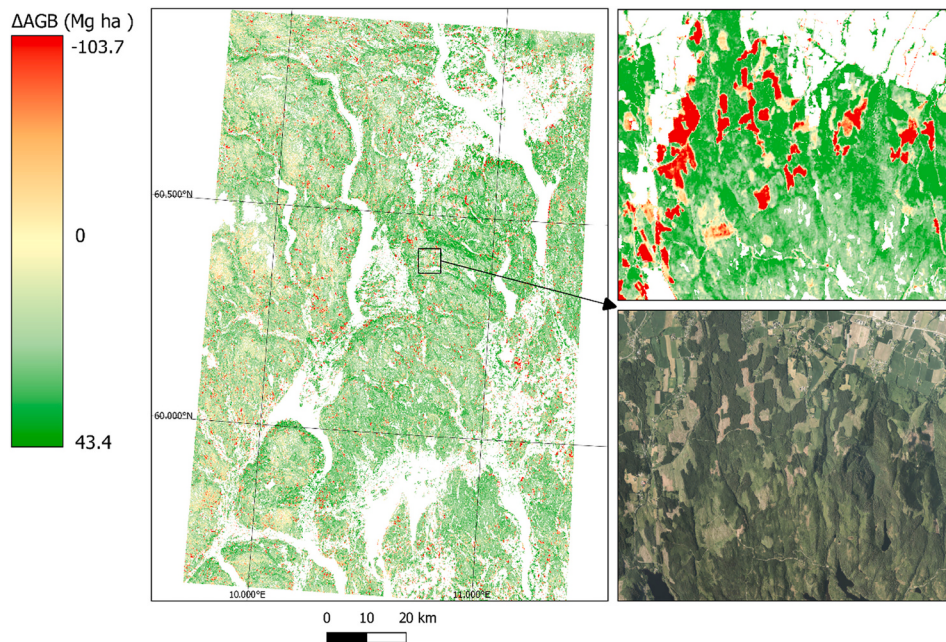


Fig. 4. Predicted ΔAGB based on the bi-temporal Sentinel-2 model over the entire and in a detailed area. Harvested areas are given in shades of red while different growth rates for forests are visible in shades of green. (For interpretation of the references to color in this figure legend, the reader is referred to the web version of this article.)

Table 4
Estimated total change in above-ground biomass ($\hat{\gamma}$; Mg).

Period of interest	Availability of remotely sensed data	BE		MA Sentinel-2		MA Landsat	
		Tot (Gg)	SE (Gg)	Tot (Gg)	SE (Gg)	Tot (Gg)	SE (Gg)
2014–2019	Bi-temporal	0.12	2.94	2.57	1.7	1.83	1.92
	Uni-temporal			1.56	1.84	2.33	2.16
2010–2015	Uni-temporal	6.12	2.36	4.51	2.03	5.87	2.04

growing forests. The proposed uni-temporal approach is therefore a potentially useful solution for those cases where remotely sensed data are limited in time or due to frequent cloud cover. Based on our results, future studies should further address the underlying causes and possible ways to mitigate the variation in the precision of ΔAGB estimates

through time.

4.3. Comparison between Sentinel-2 and Landsat data

Based on this study's results, we found that Sentinel-2 data produced more precise estimates of ΔAGB than Landsat data. This could be partly attributable to the finer spatial (Mascorro et al., 2015), spectral, and

Table 5

Relative efficiency for the model-assisted estimates of ΔAGB using either bitemporal or uni-temporal data from either Sentinel-2 or Landsat.

Period of interest	Availability of remotely sensed data	Sentinel-2	Landsat
2014–2019	Bi-temporal	2.7	2.3
	Uni-temporal	2.5	1.8
2010–2015	Uni-temporal	1.3	1.3

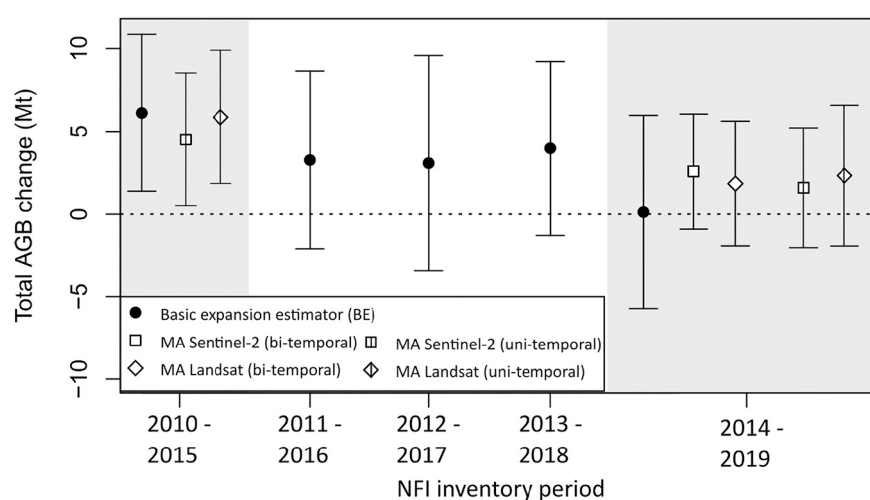


Fig. 5. Total estimated ΔAGB and 95% confidence intervals for the direct estimate and model-assisted estimates using either Sentinel-2 (MA Sentinel-2) or Landsat data (MA Landsat) and using either bi-temporal or uni-temporal mosaics. The gray bands highlight the NFI inventory periods of interest.

temporal resolution of Sentinel-2 data compared to Landsat data. In addition to data-specific differences, variations in the mosaicking methods may have affected the model fit of these two models. In particular, the Sentinel-2 mosaic was generated from summer-only acquisitions, while Landsat GLAD ARD mosaic was generated using an average from a gap-filled yearly stack of images. The latter approach may have introduced a larger variation in the reflectance values. The Sentinel-2 mosaics may have been more phenologically consistent by adopting a narrow timeframe, thus explaining the stronger model fit. Furthermore, the differences in the mosaicking algorithm may have affected different data qualities. While out of this study's scope, further research should assess how the different mosaicking methods used for different types of ARD such as the UMD ARD or the Copernicus Sentinel-2 global mosaic (Copernicus, 2020b) affect the model fit and thus the precision of the ΔAGB estimates.

Even though estimates based on Landsat data were less precise than Sentinel-2, it was encouraging to see that when using globally available ARD products (e.g., UMD ARD data), the decrease in precision compared to a custom dataset (i.e., Sentinel-2) was only marginal. The main advantage of using Landsat data in combination with NFI data is that it allows us to retroactively estimate AGB dynamics for past NFI inventory cycles, which is impossible for Sentinel-2. Thus, if Sentinel-2 may become the standard for future ΔAGB estimation (GFOI, 2020), Landsat data can form the backbone for a retroactive estimation of AGB dynamics. Further efforts should be devoted to exploring synergies between Sentinel-2 and Landsat data concerning the generation of cloud-free mosaics drawing both from Sentinel-2 and Landsat (Saunier et al., 2019; Shao et al., 2019). Such data products could benefit from the availability of a denser image time series because of the increased chances of cloud-free imagery, thus ensuring a continuous monitoring of forest AGB dynamics.

4.4. Comparison between using bi- or uni-temporal satellite data

During the 2014–2019 period, we found that there was only a small increase in precision when using bi-temporal data compared to uni-temporal data, indicating that ΔAGB could also be estimated when remotely sensed data are available only from the end of the monitoring period. A possible explanation behind such findings is that the magnitude of change in AGB is partly explained by the forest canopy's reflectance properties in the different developmental stages (AGB gain) or of harvested sites (AGB loss). The quantification of the AGB gains reflects differences in the reflectance due to the forest's phenology during different developmental stages and thus with different growth patterns. On the other hand, the possibility of estimating AGB losses might be related to variations in reflectance driven by differences in the cover and floristic compositions of post-harvest ground vegetation. This is in line with the findings by Bergstedt and Milberg (2001) who, using Swedish NFI data, found that post-harvest ground cover vegetation and floristic composition were strongly correlated to the logging intensity (i.e., extracted timber volume). The main advantages of using remotely sensed data for only the end of the monitoring period are: 1) no requirement of availability of two cloud-free mosaics, and thus increases the years for which ΔAGB estimates may be possible, and 2) retroactively estimate ΔAGB for inventory cycles before the existence of a particular data source. The latter is particularly relevant for Sentinel-2 data, which are available only since 2015, and thus only changes after 2019 can be estimated based on bi-temporal data. On the other hand, using uni-temporal Sentinel-2 data allowed us to estimate ΔAGB that occurred before 2015 (e.g., NFI cycle between 2010 and 2015).

4.5. Scalability

Our study is part of the ongoing global research effort aiming on improving methods for reliable and consistent greenhouse gas inventories in order to fully understand and utilize the climate mitigation

potential of forests. Given that Sentinel-2 were available only since 2015, the main merit of this study is to represent some of the first results to understanding how these data can be used for ΔAGB estimation at a regional scale. The extent of the study area was constrained by the availability of cloud-free Sentinel-2 data in 2015. Even though limited compared to the nationwide availability of NFI, the size of our study area ($13,659 \text{ km}^2$) remains the largest amongst other studies estimating ΔAGB such as Næsset et al. (2013), Bollandsås et al. (2013) and McRoberts et al. (2015) ($8\text{--}10 \text{ km}^2$), or even Strímbu et al. (2017) (9758 km^2). When considering the geographical scalability of the methods described in this study to broader scales, one must be aware of a potentially larger heterogeneity in the image mosaics' quality due to increased cloud cover, seasonal variations, and variations in atmospheric conditions. The increased variability in the quality of the predictor variables is likely to have a negative effect on the model fit and thus on the precision of the ΔAGB estimates. Furthermore, more complex vegetation dynamics and drivers of change can be expected when increasing the geographical extent. As seen by the comparison of the ΔAGB estimates from uni-temporal remotely sensed data in the two studied time periods, the more precise estimates were found for the 2014–2019 period during which there was a larger number of harvested areas and with larger biomass removals. This indicated that the method is more efficient in areas characterized by active forest management with substantial AGB losses compared to un-productive and set-aside areas. Of particular interest in regard to satellite imagery is the presence of biotic (e.g. bark beetle attacks) and abiotic damages (e.g. forest fire), which can substantially alter the canopy reflectance but have a limited impact on the AGB dynamics compared to forest harvest. The extensive presence of forest damages could therefore challenge the ΔAGB modeling in certain areas and thus the precision of the resulting estimates.

In this study, a probability sample of field data were available and thus we could adopt a model-assisted inferential framework, thus providing an understanding of the value of satellite imagery for ΔAGB estimation in a best-case scenario. Nevertheless, in most areas in the world probability samples with repeated AGB measurements are unavailable and therefore different methods and estimators must be adopted. In realms without repeated field measurements, the gain-loss method should be used (GFOI, 2020) according to which satellite imagery only provide the activity data regarding the land use changes.

A further aspect to consider is that we used an existing nationwide forest mask to delineate the studied population (i.e., forests) and exclude model predictions from non-forest areas. When extending our method to areas outside of Norway, there is a need for a global forest mask with consistent accuracy. Several options exist nowadays as a global source forest/non-forest maps such as the tree cover dataset for the year 2000 produced using Landsat 7 ETM (Hansen et al., 2013), the forest/non-forest map produced from TanDEM-X data (Martone et al., 2018) or the future availability of the WorldCover map at 10 m resolution (ESA, 2020). While several masks may be used, further studies should investigate the effect of using different forest masks on the estimates' precision.

The temporal scalability of the proposed method also is of interest. While we only looked at a single five-year period, the described method can be applied retroactively to improve the precision of time series of ΔAGB estimates from past inventories, thus defining more accurate baselines. In such a context, Landsat data can prove invaluable as they provide a multi-decadal time-series dating back to the 1970s. With that in mind, it remains important to acknowledge the varying data quality for the different Landsat missions.

5. Conclusion

This study is the first example of a direct model-assisted estimation of ΔAGB using freely available satellite optical data. Based on the results of this study, our conclusion is fourfold:

- The use of auxiliary data from freely available satellite imagery can boost the precision of regional field-based estimates of forest ΔAGB. Such a result is encouraging for future use alongside NFI programs to provide a more precise understanding of forests' role in the carbon cycle.
- The most precise ΔAGB estimates were found to be based on bi-temporal Sentinel-2 data, followed by the use of uni-temporal Sentinel-2 data. Even though Landsat data resulted in a smaller precision of the estimates compared to Sentinel-2, their use for improving past AGB estimates could prove to be useful.
- Uni-temporal data can be used for estimating AGB dynamics in situations where remotely sensed data may be missing at the beginning of the monitoring period.
- The ΔAGB estimates were more precise for the five-years period during which more harvested plots and with larger AGB losses occurred, indicating a better performance of the proposed methods in areas with active forest management or with larger AGB losses.

This study represents a step towards a better understanding of the value of freely available satellite imagery for the future monitoring of AGB dynamics. Our results were encouraging on a regional scale and for a specific point in time. However, there is need to understand how efficient the method is on broader scales with more diverse forest types, drivers of change, and variations in quality of the satellite imagery. In the future, the increased availability of longer and denser time-series of satellite data will allow to address the abovementioned research questions.

Declaration of Competing Interest

The authors declare that they have no known competing financial interests or personal relationships that could have appeared to influence the work reported in this paper.

Acknowledgments

We are grateful to Peter Potapov and Matthew Hansen for providing the GLAD Landsat ARD data, and to the Copernicus and Landsat programs for providing free access to their data. The Sentinel-2 data were mosaicked and provided by the Norwegian Mapping Authority (Kartverket), supported by the Norwegian Space Centre project n. NIT. 04.19.5. This study was supported by the Norwegian Institute for Bioeconomy Research (NIBIO) and ERA-GAS INVENT (NRC number 276398).

Appendix A. Supplementary data

Supplementary data to this article can be found online at <https://doi.org/10.1016/j.rse.2021.112644>.

References

- Ahlstrøm, A., Bjørkelo, K., Frydenlund, J., 2014. AR5 klassifikasjonssystem – klassifikasjon av arealressurser [AR5 classification scheme – classification of areal resources]. In: Rapport fra Skog og landskap [Norwegian].
- Astrup, R., Rahlf, J., Bjørkelo, K., Debella-Gilo, M., Gjertsen, A.-K., Breidenbach, J., 2019. Forest information at multiple scales: development, evaluation and application of the Norwegian forest resources map SR16. *Scand. J. For. Res.* 34, 484–496.
- Baccini, A., Goetz, S.J., Walker, W.S., Laporte, N.T., Sun, M., Sulla-Menache, D., Hackler, J., Beck, P.S.A., Dubayah, R., Friedl, M.A., Samanta, S., Houghton, R.A., 2012. Estimated carbon dioxide emissions from tropical deforestation improved by carbon-density maps. *Nat. Clim. Chang.* 2, 182–185.
- Bergstedt, J., Milberg, P., 2001. The impact of logging intensity on field-layer vegetation in Swedish boreal forests. *For. Ecol. Manag.* 154, 105–115.
- Bollandsås, O.M., Gregoire, T.G., Næsset, E., Øyen, B.-H., 2013. Detection of biomass change in a Norwegian mountain forest area using small footprint airborne laser scanner data. *Statist. Methods Appl.* 22, 113–129.
- Bollandsås, O.M., Ene, L.T., Gobakken, T., Næsset, E., 2018. Estimation of biomass change in montane forests in Norway along a 1200 km latitudinal gradient using airborne laser scanning: a comparison of direct and indirect prediction of change under a model-based inferential approach. *Scand. J. For. Res.* 33, 155–165.
- Breidenbach, J., Granhus, A., Hylen, G., Eriksen, R., Astrup, R., 2020a. A century of National Forest Inventory in Norway – informing past, present, and future decisions. *Forest Ecosyst.* 7, 46.
- Breidenbach, J., Waser, L.T., Debella-Gilo, M., Schumacher, J., Rahlf, J., Hauglin, M., Puliti, S., Astrup, R., 2020b. National mapping and estimation of forest area by dominant tree species using Sentinel-2 data. *Can. J. For. Res.* 51, 365–379.
- Breidenbach, J., Ivanovs, J., Kangas, A., Nord-Larsen, T., Nilsson, M., Astrup, R., 2021. Improving living biomass C-stock loss estimates by combining optical satellite, airborne laser scanning, and NFI data. *Can. J. For. Res.*
- Cohen, W.B., Yang, Z., Kennedy, R., 2010. Detecting trends in forest disturbance and recovery using yearly Landsat time series: 2. TimeSync — Tools for calibration and validation. *Remote Sens. Environ.* 114, 2911–2924.
- Copernicus, 2020. Copernicus Open Access Hub.
- Copernicus, 2020b. S2GM User Manual In Copernicus.
- Csillik, O., Kumar, P., Mascaro, J., O'Shea, T., Asner, G.P., 2019. Monitoring tropical forest carbon stocks and emissions using planet satellite data. *Sci. Rep.* 9, 17831.
- Drusch, M., Del Bello, U., Carlier, S., Colin, O., Fernandez, V., Gascon, F., Hoersch, B., Isola, C., Laberinti, P., Martimort, P., Meygret, A., Spoto, F., Sy, O., Marchese, F., Bargellini, P., 2012. Sentinel-2: ESA's optical high-resolution Mission for GMES operational services. *Remote Sens. Environ.* 120, 25–36.
- Duncanson, L., Armston, J., Disney, M., Avitabile, V., Barbier, N., Calders, K., Carter, S., Chave, J., Herold, M., Crowther, T.W., Falkowski, M., Kellner, J.R., Labrière, N., Lucas, R., MacBean, N., McRoberts, R.E., Meyer, V., Næsset, E., Nickeson, J.E., Paul, K.I., Phillips, O.L., Réjou-Méchain, M., Román, M., Roxburgh, S., Saatchi, S., Schepaschenko, D., Scipal, K., Siqueira, P.R., Whitehurst, A., Williams, M., 2019. The importance of consistent global Forest aboveground biomass product validation. *Surv. Geophys.* 40, 979–999.
- Duncanson, L., Armston, J., Disney, M., Avitabile, V., Barbier, N., Calders, K., Carter, S., Chave, J., Herold, M., MacBean, N., McRoberts, R., Minor, D., Paul, K., Réjou-Méchain, M., Roxburgh, S., Williams, M., Albinet, C., Baker, T., Bartholomew, H., Bastin, J.-F., Coomes, D., Crowther, T., Davies, S., de Bruin, S., De Kauwe, M., Domke, G., Dubayah, R., Falkowski, M., Fatoyinbo, L., Goetz, S., Jantz, P., Jonckheere, I., Jucker, T., Kay, H., Kellner, J., Labrière, N., Lucas, R., Mitchard, E., Morsdorf, F., Næsset, E., Park, T., Phillips, O., Ploton, P., Puliti, S., Quegan, S., Saatchi, S., Schaaf, C., Schepaschenko, D., Scipal, K., Stovall, A., Thiel, C., Wulder, M.A., Camacho, F., Nickeson, J., Román, M., Margolis, H., 2021. Aboveground Woody biomass product validation good practices protocol. In: Duncanson, L., Disney, M., Armston, J., Nickeson, J., Minor, D., Camacho, F. (Eds.), Good Practices for Satellite Derived Land Product Validation (Pp. 1–236): CEOS Working Group on Calibration and Validation (Lanf Product Validation Subgroup).
- Eggleston, H.S., Buendia, L., Miwa, K., Ngara, T., Tanabe, K., 2006. 2006 IPCC Guidelines for National Greenhouse Gas Inventories.; IPCC National Greenhouse Gas Inventories Programme, Intergovernmental Panel on Climate Change IPCC, c/o Institute for Global Environmental Strategies IGES, 2108–11, Kamiyamaguchi, Hayama, Kanagawa (Japan).
- Ene, L.T., Næsset, E., Gobakken, T., Bollandsås, O.M., Mauya, E.W., Zahabu, E., 2017. Large-scale estimation of change in aboveground biomass in miombo woodlands using airborne laser scanning and national forest inventory data. *Remote Sensing of Environment* 188, 106–117.
- ESA, 2020. WorldCover.
- Fuller, R.M., Smith, G.M., Devereux, B.J., 2003. The characterisation and measurement of land cover change through remote sensing: problems in operational applications? *Int. J. Appl. Earth Obs. Geoinf.* 4, 243–253.
- Gascon, F., Bouzinac, C., Thépaut, O., Jung, M., Francesconi, B., Louis, J., Lonjou, V., Lafrance, B., Massera, S., Gaudel-Vacaresse, A., Languielle, F., Alhammoud, B., Viallefond, F., Pfugl, B., Bieniarz, J., Clerc, S., Pessiot, L., Trémass, T., Cadau, E., De Bonis, R., Isola, C., Martimort, P., Fernandez, V., 2017. Copernicus sentinel-2A calibration and products validation status. *Remote Sens.* 9, 584.
- GFOI, 2013. In: Observations, G.O.E. (Ed.), Integrating Remote-Sensing and Ground-Based Observations for Estimation of Emissions and Removals of Greenhouse Gases in Forests: Methods and Guidance from the Global Forest Observations Initiative. Switzerland, Geneva.
- GFOI, 2020. Integration of remote-sensing and ground-based observations for estimation of emissions and removals of greenhouse gases in forests. In: Initiative, G.F.O. (Ed.), Methods and Guidance from the Global Forest Observations Initiative.
- Glad, U., 2020. GLAD Landsat ARD Tools.
- Gregoire, T.G., 1998. Design-based and model-based inference in survey sampling: appreciating the difference. *Can. J. For. Res.* 28, 1429–1447.
- Hansen, M.C., Potapov, P.V., Moore, R., Hancher, M., Turubanova, S.A., Tyukavina, A., Thau, D., Stehman, S.V., Goetz, S.J., Loveland, T.R., Kommareddy, A., Egorov, A., Chini, L., Justice, C.O., Townshend, J.R.G., 2013. High-resolution global maps of 21st-century Forest cover change. *Science* 342, 850–853.
- Harris, N.L., Gibbs, D.A., Baccini, A., Birdsey, R.A., de Bruin, S., Farina, M., Fatoyinbo, L., Hansen, M.C., Herold, M., Houghton, R.A., Potapov, P.V., Suarez, D.R., Roman-Cuesta, R.M., Saatchi, S.S., Slay, C.M., Turubanova, S.A., Tyukavina, A., 2021. Global maps of twenty-first century forest carbon fluxes. *Nat. Clim. Chang.* 11, 234–240.
- Herold, M., Carter, S., Avitabile, V., Espejo, A.B., Jonckheere, I., Lucas, R., McRoberts, R. E., Næsset, E., Nightingale, J., Petersen, R., Reiche, J., Romijn, E., Rosenqvist, A., Rozendaal, D.M.A., Seifert, F.M., Sanz, M.J., De Sy, V., 2019. The role and need for space-based Forest biomass-related measurements in environmental management and policy. *Surv. Geophys.* 40, 757–778.
- IPCC, 2019. 2019 Refinement to the 2006 IPCC Guidelines for National Greenhouse Gas Inventories. In: Calvo Buendia, E., Tanabe, K., Kranjc, A., Baasansuren, J.,

- Fukuda, M., Ngarize, S., Osako, A., Pyrozhenko, Y., Shermanau, P., Federici, S. (Eds.). Published: IPCC, Switzerl.
- Karila, K., Yu, X., Vastaranta, M., Karjalainen, M., Puttonen, E., Hyppä, J., 2019. TanDEM-X digital surface models in boreal forest above-ground biomass change detection. *ISPRS J. Photogramm. Remote Sens.* 148, 174–183.
- Laurin, G.V., Balling, J., Corona, P., Mattioli, W., Papale, D., Puletti, N., Rizzo, M., Truckenbrodt, J., Urban, M., 2018. Above-ground biomass prediction by Sentinel-1 multitemporal data in Central Italy with integration of ALOS2 and Sentinel-2 data. *J. Appl. Remote. Sens.* 12, 016008.
- Li, Y., Li, M., Li, C., Liu, Z., 2020. Forest aboveground biomass estimation using Landsat 8 and sentinel-1A data with machine learning algorithms. *Sci. Rep.* 10, 9952.
- Main-Knorn, M., Cohen, W.B., Kennedy, R.E., Grodzki, W., Pfugmacher, D., Griffiths, P., Hostert, P., 2013. Monitoring coniferous forest biomass change using a Landsat trajectory-based approach. *Remote Sens. Environ.* 139, 277–290.
- Marklund, L.G., 1988. Biomass functions for pine, spruce and birch in Sweden. In: Rapport-Sveriges Lantbruksuniversitet, Institutionen foer Skogstaxering (Sweden). Swedish University of Agricultural Sciences, Umeå.
- Martone, M., Rizzoli, P., Wecklich, C., González, C., Bueso-Bello, J.-L., Valdo, P., Schulze, D., Zink, M., Krieger, G., Moreira, A., 2018. The global forest/non-forest map from TanDEM-X interferometric SAR data. *Remote Sens. Environ.* 205, 352–373.
- Mascorro, V.S., Coops, N.C., Kurz, W.A., Olgún, M., 2015. Choice of satellite imagery and attribution of changes to disturbance type strongly affects forest carbon balance estimates. *Carbon Bal. Manage.* 10, 30.
- Matasci, G., Hermosilla, T., Wilder, M.A., White, J.C., Coops, N.C., Hobart, G.W., Bolton, D.K., Tompalski, P., Bater, C.W., 2018. Three decades of forest structural dynamics over Canada's forested ecosystems using Landsat time-series and lidar plots. *Remote Sens. Environ.* 216, 697–714.
- McRoberts, R.E., Næsset, E., Gobakken, T., Bollandsås, O.M., 2015. Indirect and direct estimation of forest biomass change using forest inventory and airborne laser scanning data. *Remote Sens. Environ.* 164, 36–42.
- McRoberts, R.E., Næsset, E., Sannier, C., Stehman, S.V., Tomppo, E.O., 2020. Remote sensing support for the gain-loss approach for greenhouse gas inventories. *Remote Sens.* 12, 1891.
- Næsset, E., Bollandsås, O.M., Gobakken, T., Gregoire, T.G., Ståhl, G., 2013. Model-assisted estimation of change in forest biomass over an 11year period in a sample survey supported by airborne LiDAR: a case study with post-stratification to provide “activity data”. *Remote Sens. Environ.* 128, 299–314.
- Næsset, E., Bollandsås, O.M., Gobakken, T., Solberg, S., McRoberts, R.E., 2015. The effects of field plot size on model-assisted estimation of aboveground biomass change using multitemporal interferometric SAR and airborne laser scanning data. *Remote Sens. Environ.* 168, 252–264.
- Nguyen, T.H., Jones, S.D., Soto-Berelov, M., Haywood, A., Hislop, S., 2020. Monitoring aboveground forest biomass dynamics over three decades using Landsat time-series and single-date inventory data. *Int. J. Appl. Earth Obs. Geoinf.* 84, 101952.
- Potapov, P., Hansen, M.C., Komiareddy, I., Komiareddy, A., Turubanova, S., Pickens, A., Adusei, B., Tyukavina, A., Ying, Q., 2020. Landsat analysis ready data for global land cover and land cover change mapping. *Remote Sens.* 12, 426.
- Powell, S.L., Cohen, W.B., Healey, S.P., Kennedy, R.E., Moisen, G.G., Pierce, K.B., Ohmann, J.L., 2010. Quantification of live aboveground forest biomass dynamics with Landsat time-series and field inventory data: a comparison of empirical modeling approaches. *Remote Sens. Environ.* 114, 1053–1068.
- Price, B., Waser, L.T., Wang, Z., Marty, M., Ginzler, C., Zellweger, F., 2020. Predicting biomass dynamics at the national extent from digital aerial photogrammetry. *Int. J. Appl. Earth Obs. Geoinf.* 90, 102116.
- Puliti, S., Hauglin, M., Breidenbach, J., Montesano, P., Neigh, C.S.R., Rahlf, J., Solberg, S., Klingenberg, T.F., Astrup, R., 2020. Modelling above-ground biomass stock over Norway using national forest inventory data with ArcticDEM and Sentinel-2 data. *Remote Sens. Environ.* 236, 111501.
- Särndal, C.E., 1984. Design-consistent versus model-dependent estimation for small domains. *J. Am. Stat. Assoc.* 79, 624–631.
- Saunier, S., Louis, J., Debaecker, V., Beaton, T., Cadau, E.G., Boccia, V., Gascon, F., 2019. Sen2like, A Tool To Generate Sentinel-2 Harmonised Surface Reflectance Products - First Results with Landsat-8. In: IGARSS 2019–2019 IEEE International Geoscience and Remote Sensing Symposium (pp. 5650–5653).
- Shao, Z., Cai, J., Fu, P., Hu, L., Liu, T., 2019. Deep learning-based fusion of Landsat-8 and Sentinel-2 images for a harmonized surface reflectance product. *Remote Sens. Environ.* 235, 111425.
- Skowronski, N.S., Clark, K.L., Gallagher, M., Birdsey, R.A., Hom, J.L., 2014. Airborne laser scanner-assisted estimation of aboveground biomass change in a temperate oak-pine forest. *Remote Sens. Environ.* 151, 166–174.
- Solberg, S., Næsset, E., Gobakken, T., Bollandsås, O.-M., 2014. Forest biomass change estimated from height change in interferometric SAR height models. *Carbon Bal. Manage.* 9, 5.
- Ståhl, G., Saarela, S., Schnell, S., Holm, S., Breidenbach, J., Healey, S.P., Patterson, P.L., Magnussen, S., Næsset, E., McRoberts, R.E., Gregoire, T.G., 2016. Use of models in large-area forest surveys: comparing model-assisted, model-based and hybrid estimation. *Forest Ecosyst.* 3, 5.
- Strimbu, V.F., Ene, L.T., Gobakken, T., Gregoire, T.G., Astrup, R., Næsset, E., 2017. Post-stratified change estimation for large-area forest biomass using repeated ALS strip sampling. *Can. J. For. Res.* 47, 839–847.
- White, J.C., Saarinen, N., Kankare, V., Wulder, M.A., Hermosilla, T., Coops, N.C., Pickell, P.D., Holopainen, M., Hyppä, J., Vastaranta, M., 2018. Confirmation of post-harvest spectral recovery from Landsat time series using measures of forest cover and height derived from airborne laser scanning data. *Remote Sens. Environ.* 216, 262–275.
- Wulder, M.A., Masek, J.G., Cohen, W.B., Loveland, T.R., Woodcock, C.E., 2012. Opening the archive: how free data has enabled the science and monitoring promise of Landsat. *Remote Sens. Environ.* 122, 2–10.
- Wulder, M.A., Hermosilla, T., White, J.C., Coops, N.C., 2020. Biomass status and dynamics over Canada's forests: disentangling disturbed area from associated aboveground biomass consequences. *Environ. Res. Lett.* 15, 094093.
- Zolkos, S.G., Goetz, S.J., Dubayah, R., 2013. A meta-analysis of terrestrial aboveground biomass estimation using lidar remote sensing. *Remote Sens. Environ.* 128, 289–298.